Heliyon 11 (2025) e41636

Contents lists available at ScienceDirect

Heliyon

journal homepage: www.cell.com/heliyon

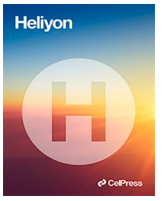

Research article

In-vitro study of hybrid silver nanoparticles with humic acid extracted from cow dung against pathogens

Shabir Ahmed Dharejo [a], Tajnees Pirzada [a,**], Muhammad Raza Shah [b], Ahmed Nadeem [c], Khalid Hussain Thebo [d,*]

[a] Institute of Chemistry, Shah Abdul Latif University, Khairpur Mir's, 66020, Sindh, Pakistan
[b] International Center for Chemical and Biological Sciences, H.E.J. Research Institute of Chemistry, Karachi University Karachi, 74200, Pakistan
[c] Department of Pharmacology and Toxicology, College of Pharmacy, King Saud University, Riyadh, 11451, Saudi Arabia
[d] Institute of Metal Research (IMR), Chinese Academy of Science, Wenhua Road, Shenyang, China

ARTICLE INFO

Keywords:
Silver nanoparticles
Cow dung
Humic acid
Coupled
Antimicrobial activities

ABSTRACT

Recently, researchers have used silver nanoparticles (AgNPs) coupled with humic acid (HA) as antimicrobial agents. Herein, AgNPs were prepared and coupled with humic acid for their antimicrobial activities. The as-prepared AgNPs coupled with humic acid (HA) were characterized by an atomic force microscope (AFM), X-ray powder diffraction (XRD), zeta potential, zeta sizer, Fourier-transform infrared (FT-IR) spectroscopy, and UV–VIS spectrophotometer. Moreover, human plasma, varied salt concentrations, and pH levels were used for stability confirmation using a UV–VIS spectrophotometer. The antibacterial activities and minimal bactericidal concentration (MBC) of coupled AgNPs were determined by disk diffusion and broth dilution methods, respectively, against identified *Staphylococcus aureus, Streptococcus pyogene, Pseudomonas aeruginosa,* and *Escherichia coli*, which are extracted from cow dung. AgNPs' peak in the UV–Vis spectral range showed maximal absorption at 415 nm. The coupled AgNPs displayed their distinctive peak under all circumstances, demonstrating their stability. The FT-IR displayed functional groups such as hydroxyl, carboxylic acids, carbonyl, ester, and ether groups. The particles were face-centered cubic (FCC) in structure, according to the XRD. Moreover, particles had a spherical shape, high negative zeta potential, and were polydisperse in nature, with an average size of 25.43 nm. The minimal bactericidal concentration (MBC) of AgNPs was found to be 2.5 mg/mL, and the MBC of AgNPs/HA was found to be 5 mg/mL. The result indicated that the as-synthesizedAgNPs/HA are more effective in inhibiting all the studied microorganisms, which can be attributed to the therapeutic use of nanoparticles coated with humic acids.

1. Introduction

Humic acid (HA) is a complex mixture and inexpensive source for novel multifunctional materials for a huge range of applications. But the aggregation and degradation phenomena in different environments do allow their complete development and utilization [1,2]. Hence, a suitable planning is required to resolve these issues, depending on combining HA moieties at the molecular scale with

* Corresponding author.
** Corresponding author.
E-mail addresses: tajnees@yahoo.com (T. Pirzada), khalidthebo@yahoo.com (K.H. Thebo).

https://doi.org/10.1016/j.heliyon.2025.e41636
Received 23 September 2024; Received in revised form 31 December 2024; Accepted 2 January 2025
Available online 3 January 2025

inorganic nanostructured components, leading to more stable hybrid nanomaterials with various functionalities [3–5]. The structure of HA is believed to be composed of various molecules held together by hydrophobic interactions and hydrogen bonds. However, the exact structure of HA can vary depending on factors such as the source of organic matter, the extraction methods, and environmental conditions during decomposition [6,7]. HA has a broad series of applications in different fields. In agriculture, it is used to promote the growth and production of important substances in medicinal plants. Additionally, HA has been explored as an antimicrobial cause in medicine and utilized in the protection of the environment [8–10].

Recently, metal-based nanoparticles (M − B NPs) have attracted significant attention due to their biomedical applications [11–14]. They have been found to be effective against pathogens, as recognized by the World Health Organization (WHO). The increasing demand for nanotechnology and nanoscale materials in clinical applications, particularly for the healing of infectious diseases, has led to the investigation of M − B NPs as potential antimicrobial agents [15]. The emergence of bacterial resistance has created the dire a need for alternative and effective antimicrobial approaches [16]. Nanoparticles have shown antimicrobial activity by targeting crucial molecular pathways within pathogenic microorganisms [17–20]. Especially, AgNPs possess beneficial biological properties [21] that make them highly valuable in the prevention of various infections in chronic and non-healing wounds among diabetic patients [11]. The unique properties and biocompatibility of biosynthesized AgNPs have drawn a lot of attention as potential nanocarriers in biomedical applications. The biosynthesis process uses biological entities like plants, bacteria, or fungi to create the nanoparticles, which can have a number of advantages over traditional chemical synthesis methods [22,23]. Biosynthesized AgNPs are often less toxic and more biocompatible than chemically synthesized ones because the biological molecules used in the synthesis can cap the nanoparticles, stabilizing them and lowering their potential toxicity. Silver nanoparticles (AgNPs) were synthesized using physical, chemical, biological, and hybrid processes, and each method has unique benefits and uses [24,25]. Physical methods include procedures like laser ablation and evaporation-condensation. High-purity nanoparticles are frequently produced via physical processes; however, they may need costly equipment and significant energy input. While chemical reduction is one of the popular chemical methods in terms of simplicity and cost. In which different green reducing agents, such as citrate or sodium borohydride, are used to reduce silver ions [25,26]. Further, biological methods involve the conversion of silver ions to nanoparticles by using biological agents including bacteria, fungus, algae, and plant extracts. Although biological synthesis might be slower, it is generally ecologically benign and produces biocompatible nanoparticles.

Then, the hybrid method involves combining components from several production processes. For instance, combining chemical and biological approaches can improve the reduction process and efficiently stabilize nanoparticles. There are several advantages of these technique for coating AgNPs with HA over alternative approaches. In this way, the stability of the nanoparticles is greatly increased by using HA as a capping agent. Because HA is both biocompatible and bioactive, it may be used in biomedical applications, such antimicrobial treatments, medication transport, and bone tissue creation. By using these qualities of HA, this capping technique produces nanoparticles that are safer and more useful for use in medical applications. The approach outlined is comparatively uncomplicated and doesn't call for intricate tools or steps. This technique is accessible and repeatable in typical laboratory settings due to the use of basic laboratory chemicals ($AgNO_3$, $NaBH_4$, and ethanol) and a straightforward drying procedure at 60 °C. Ethanol and filtration are used in the purification process to effectively remove contaminants and unreacted elements from the finished product. This process is essential for applications where the nanoparticles' purity is vital [27,28]. Depending on how many nanoparticles are needed, the procedure can be readily scaled up or down. Both small-scale laboratory research and larger-scale industrial manufacturing benefit from this flexibility. The procedure makes it possible to regulate the nanoparticles' size and distribution, which is crucial for customizing their characteristics for certain uses [29–31]. A consistent layer of HA on the AgNPs is guaranteed by the rigorous mixing and shaking procedures.

In this work, AgNPs were prepared and used to study the antibacterial effects of NPs combined with HA against *Staphylococcus, Streptococcus, E. coli, Pseudomonas, and Typhi,* which are commonly associated with skin infections. Further, different techniques such as transmission electron microscopy, X-ray photoelectron spectroscopy, UV–Vis spectroscopy, X-ray diffraction, and high-resolution transmission electron microscopy were utilized to characterize the AgNPs. Additionally, the in-vitro stability of the hybridized nanoparticles under optimized conditions, such as salt, pH, and exposure to blood plasma, was investigated. We hope this article will provide timely guidance to the scientific community.

2. Materials and methods

2.1. Chemicals and instruments

All chemicals, including sodium borohydride (NaBH4), silver nitrate (AgNO3), NaOH, and HCl, were purchased from Sigma-Aldrich (China) with MS-grade purity. Mueller Hinton broth and nutrient agar were obtained from Oxoid (UK). Deionized water was used for all experiments. The laboratory was equipped with necessary glassware and instruments, including beakers, pH meters, mechanical shakers, centrifuge machines, incubators, spectrophotometers, FT-IR (Shimadzu, Kyoto), XRD, and AFM.

2.2. Sampling Site and study area

Cow dung samples were collected from a cattle farm located in Wahi Ghoto, District Ghotki. The samples were then air-dried at 25 °C for one week, followed by grinding into a fine powder. The powdered samples were stored in airtight plastic bags, awaiting further processing and HA extraction.

2.3. Extraction and characterization of humic acid

Humic acid (HA) was extracted from cow dung samples using the standard IHSS method [32]. 100 g of sample was treated with 0.5 M NaOH and shaken at 150 rpm for 5 h, followed by a 24-h incubation at room temperature. After that, the resulting mixture was then centrifuged (5000 rpm), filtered, and acidified to facilitate HA precipitation. The precipitated HA was purified using 0.1 M HF to remove mineral impurities [33]. The extracted HA was characterized using UV–vis and FT-IR spectrophotometry.

2.4. Hybridization of silver nanoparticles with humic acid

The coating of AgNPs with HA was achieved through a multi-step process. Initially, a solution of AgNO3 and HA was mixed and stirred at 37 °C for 50–60 min. Subsequently, a fresh solution of NaBH4 was added to the reaction mixture and shaken thoroughly for 12 h. The resulting solution was then purified by adding ethanol and the solution was filtered. Finally, the filtered solution was dried at 60 °C for 25 min. The stability of the HA-coated AgNPs was evaluated after 90 days [34].

2.5. Characterization of materials

The confirmation of hybridization was achieved through the utilization of UV–VIS and FT-IR spectroscopy techniques. AFM images of AgNPs/HA were obtained to assess their morphological changes. The Nano surf Easy Scan 2 Basic Instrument AFM was used in contact mode for AFM imaging (SC Instruments, Les Ulis, France). The AFM images allowed for the measurement of AgNPs/HA' dimensions, HA's characteristics, and surface shape. Then, zeta sizer measurements were conducted to determine the typical size of the nanoparticles. The zeta sizer instrument was utilized for conducting the measurements. X-ray diffraction (XRD, D/MAX/2400, CuKα radiation, λ-0.154 nm) was utilized to analyze the XRD spectra.

2.6. Stability of hybridized silver nanoparticles using UV–VIS spectrophotometer

The stability of AgNPs/HA was investigated in various environments, including different salt concentrations, pH levels, and human blood plasma. To examine the stability of AgNPs/HA in varying salt concentrations, the nanoparticles were incubated with NaCl solutions (0.125–3 mM) in a 1:1 vol ratio for 2 h. A control sample was prepared by diluting the nanoparticle solution with DI water to provide a basis for comparison.

The stability of AgNPs/HA was assessed at different pH levels, ranging from 4 to 12. The pH of the nanoparticle solution was adjusted using concentrated HCl and NaOH solutions, and the mixture was incubated for 2 h. A control sample was prepared by diluting the nanoparticle solution with DI water.

Additionally, the stability of AgNPs/HA in human blood plasma was investigated by adding diluted plasma to the nanoparticle solution. To assess the stability of AgNPs/HA in human blood plasma, a diluted plasma solution (1:5 with DI water) was added to the AgNPs/HA solution. The absorbance was measured at various time intervals (0.5–24 h) using a UV–VIS spectrophotometer. A control sample was prepared by diluting the AgNPs/HA solution with DI water, following the same procedure.

The stability was monitored by measuring the absorbance at different time intervals using a UV–VIS spectrophotometer, which provided valuable insights into the stability of AgNPs/HA in different environments.

2.7. Anti-microbiological activities

Using the disk diffusion and broth macro dilution procedures, the antibacterial properties of AgNPs and AgNPs/HA against *Staphylococcus, Streptococcus, E. coli, Pseudomonas,* and *S. Typhi* were evaluated. The minimum inhibitory concentration (MIC) and minimum bactericidal concentration (MBC) of the nanoparticles were calculated using the broth macro dilution method, and the zone of inhibition was evaluated using the disk diffusion method.

2.7.1. Disk diffusion method

The antibacterial testing using the disk diffusion method involved the uniform spreading of *Staphylococcus aureus, Streptococcus pyogenes, Escherichia coli, Pseudomonas aeruginosa, Salmonella enterica serovar Typhi (commonly referred to as Salmonella Typhi)* bacteria onto the Muller Hinton agar's surface (MHA) plates. Disks of filter paper with varied concentrations include those with 0.156 mg/mL, 0.312 mg/mL, 0.625 mg/mL, 1.25 mg/mL, and 2.5 mg/mL. The bacterial lawn in the MHA plates was then treated with 5 mg/mL of the antimicrobial agent (AgNPs and AgNPs/HA). The agar plates were subsequently incubated in an incubator for 24 h. By measuring the zones of inhibition surrounding the filter paper disks, the antimicrobial agents' effectiveness at inhibiting bacterial growth was determined [35].

2.7.2. Broth dilution method

The MIC and MBC of the antibacterial drugs were calculated using the broth dilution method. Firstly, a standardized suspension of the test pathogen was prepared at a 0.5 McFarland scale. Next, a series of dilutions of the antimicrobial agents (AgNPs, and AgNPs/HA) were prepared and added to liquid growth culture media in tubes. Each tube was then incubated under suitable conditions. The MBC was defined as the lowest concentration of the antimicrobial agent that caused a decrease in the number of microbes, whereas the MIC was defined as the lowest concentration of the antimicrobial agent that caused no discernible microbe growth.

3. Result and discussions

3.1. Extraction and physicochemical characterization

Using the IHSS method, 10 g of humic acid (HA) was extracted from 100 g of air-dried cow dung powder. The extracted HA was characterized using a UV–vis spectrophotometer, revealing a maximum absorbance (lambda max) at 316 nm (Fig. 1a). This value matched the lambda max of the standard sample (Fig. 1b), confirming the reliability and consistency of the extracted HA.

Further, extracted HA was also characterized by FT-IR spectrometer (Fig. 1c and d). Significant absorption bands in the region of 3400 to 2900 cm^{-1}, which are attributable to OH and NH stretching, were found in the FT-IR spectrum study of HA. At 2929 cm^{-1}, a significant peak was seen, showing C-H stretching in the CH_2 and CH_3 groups. Two bands were found between 1598 and 1507 cm^{-1}, which are connected to a variety of vibrations, including the C=O, C=C, and C-C skeletal vibrations of aromatic quinones, the NH deformation, the C=N stretching, and/or H-bonded conjugated ketones. Additional peaks at 1420 cm^{-1} were seen, showing CH_2 and CH_3 group C-H bending, COO- anti symmetric stretching, OH deformation, and phenolic OH C-O stretching. The existence of aryl ethers and phenols along their C-O axes was indicated by a peak at 1217 cm^{-1}. The findings of this study demonstrate the presence of specific functional groups within the isolated HA that correspond to those described in the literature. This confirms the authenticity of the isolated HA sample, indicating that it possesses the expected chemical properties and characteristics this study bear resemblance to the research conducted by Barančíková and coworkers as both studies identified significant absorption peaks in the FT-IR analysis of humic acid [36]. A strong intensity peak at 1034 cm^{-1} was identified, which is related to polysaccharides C-OH stretching of aliphatic O-H [36]. And all these characteristics peaks were also found in resemblance with standard HA (Aldrich).

Then, FT-IR measurements were again conducted on freeze-dried samples to investigate the potential relations between Ag and HA, which could be accountable for the production and stabilization of AgNPs (Fig. 2a and b). The spectra of HA and AgNPs/HA were compared. It was observed that the absorption peaks corresponding to OH and C=O elongation exhibited slight modifications. This indicates that HA bonded with AgNPs through its carboxyl and hydroxyl group of phenol causing these functional groups to be absorbed on then nanoparticle's surface. These interactions play vital role in the synthesis and stabilization of the silver nanoparticles. These findings also supported by reported studies in literature [37–39]. Fig. 2c and d showed the AgNPs coated with HA exhibited a slight shift towards longer wavelengths, resulting in a rightward displacement of the absorption band. The wavelength (ʎ) changed from 394 nm to 414 nm, and the absorbance peak showed a decrease in intensity. These findings imply that the addition of HA during the synthesis process caused the NPs to grow or aggregate, increasing their size. For AgNPs coated with HA, Dantas et al. [40] observed a similar displacement of the plasmonic band to the right, indicating an increase in particle size brought on by the HA coating. In the case of chemical synthesis techniques, numerous researchers have shown that employing $NaBH_4$, the absorption peak of AgNPs is between 398 and 406 nm at 65 °C. It has been reported that when the M. wightiana extract is used as a reducing agent for a reaction, the reaction's absorption peak is found at 434 nm after 120 min [41].

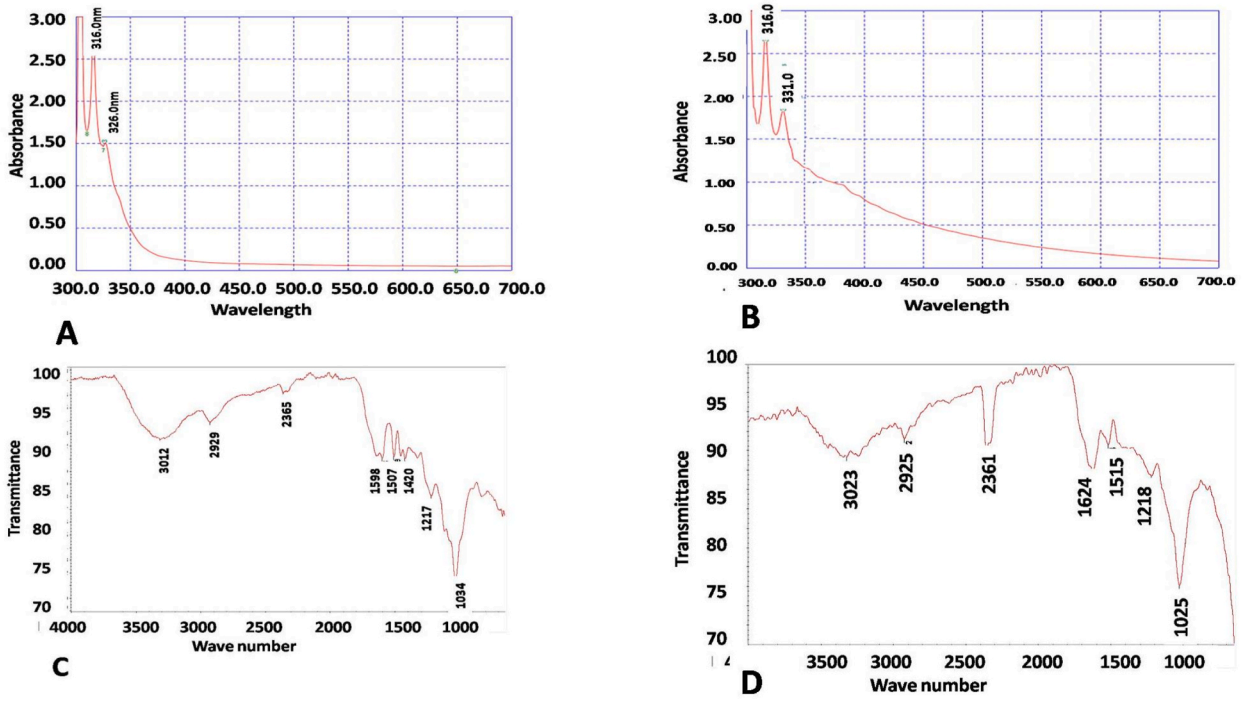

Fig. 1. (a,b) UV–vis spectra and (c,d) FT-IR spectra of isolated and standard HA, respectively.

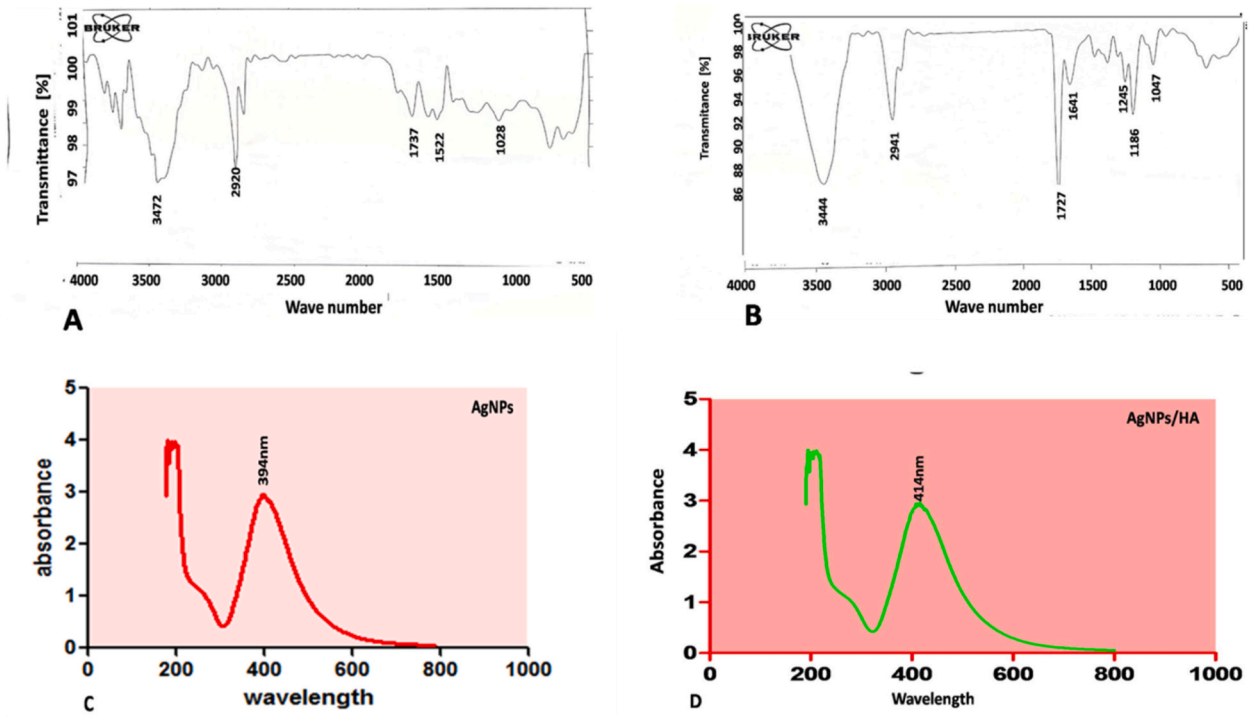

Fig. 2. (a,b) FT-IR spectra of AgNPs and AgNPs/HA, respectively, show corresponding peak to OH and C=O elongation indicates HA interact HA with AgNPs. (c,d) UV–VIS spectra of AgNPs and AgNPs/HA, respectively.

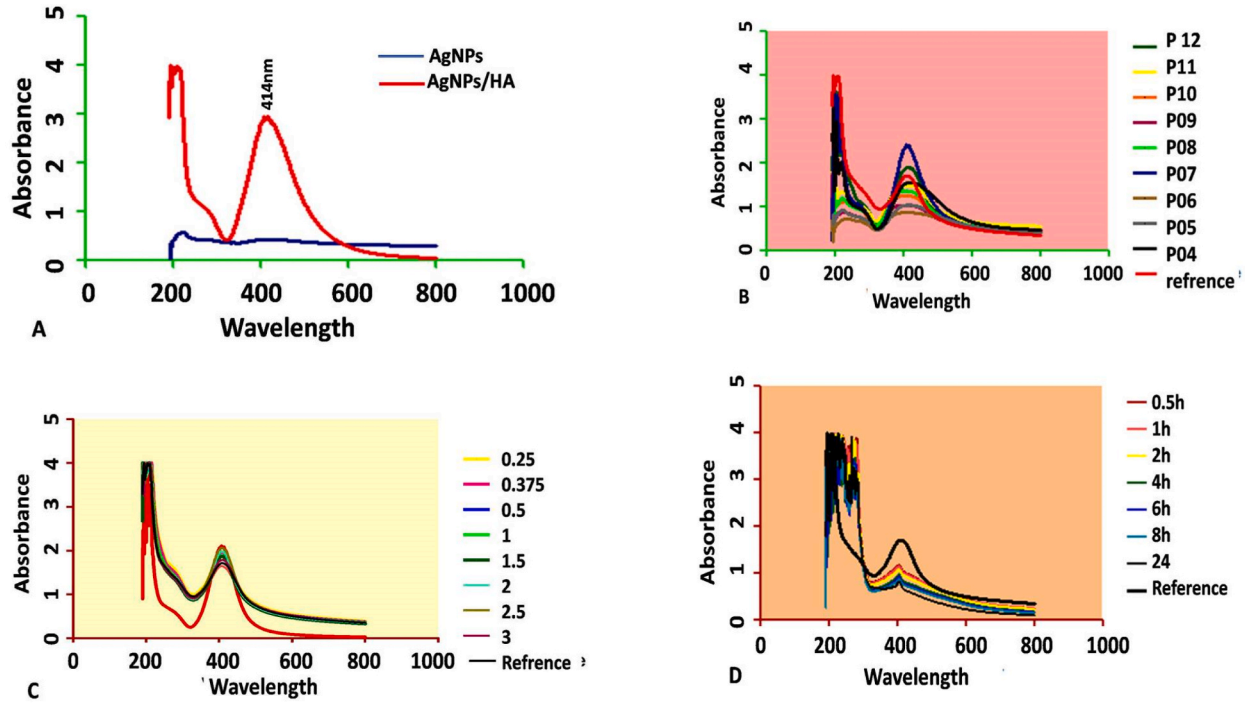

Fig. 3. (a–d) UV–VIS spectra of AgNPs/HA after 90 days at different pH, in blood plasma after different time periods, in different concentration of salt (NaCl) respectively shows same characteristic peaks at 394 nm indicate stability of AgNPs/HA.

Fig. 3a depicts the stability comparison between samples AgNPs/HA and generated solely with sodium borohydride ($NaBH_4$). The AgNPs/HA samples exhibited stability over a period of 90 days, while the AgNPs synthesized using only $NaBH_4$ showed lower stability. The improved stability of the AgNPs/HA samples can be attributed to the surface modification provided by HA. The UV–vis spectrophotometer used to measure the absorbance and other relevant parameters of the samples, indicating their stability over time. The stability of green AgNPs was also studied by several researchers [42], after different interval of time till one year and found stable. Further it was observed that all incubated samples of AgNPs/HA at different pH levels, at different concentration of salt and in human blood plasma as well as references AgNPs/HA, exhibited the same lambda maximum (Fig. 3). This suggests that the AgNPs/HA remained stable across the pH range of 4–12, even in the presence of different salt concentrations and stable in human blood plasma for up to 24 h. The stability of the nanoparticles was not compromised by the presence of human blood plasma, different concentration of salt and at different pH levels. The stability determination of AgNPs/HA in blood plasma, at different pH and at different concentration of salt by UV–vis spectroscopy it is the novelty of this study, as they retained their characteristic properties throughout the duration of the study.

The analysis revealed that AgNPs/HA exhibited a spherical form. The morphology of AgNPs was found to undergo significant modifications after being fabricated with HA. The results indicated that the average size of the AgNPs/HA fell within the range of approximately 25 nm (Fig. 4). Zeta sizer analysis was used to measure AgNPs/HA's size and yield useful data on the distribution of their particle sizes. The size of the AgNPs/HA was measured about 25.43 nm. Additionally, the poly dispersity index (PDI) value was determined to be 0.19. A low PDI value suggests a narrow particle size distribution, indicating that the synthesized AgNPs/HA are of the same type and relatively uniform in size (Fig. 4). This study measured a smaller size for the AgNPs/HA (25.43 nm) compared to the z-average hydrodynamic diameter (101.4 nm) reported in literature [40,43]. It suggests a significant difference in the size estimation between the two studies. Both studies reported PDI values, with current study showing a lower PDI (0.19) compared to the value (0.4470). A lower PDI indicates a narrower particle size distribution and greater uniformity in size. It was also reported that the Z-average size was about 105 nm with a polydispersity index of 0.297. TEM showed particle size of 11–30 nm. It is important to note that different techniques and methodologies can yield varying results in particle size analysis [44].

3.2. Zeta potential of AgNPs/HA

The results of the analysis revealed that the zeta potential of the colloidal particles was measured to be −16.7 mV (Fig. 5). A higher zeta potential indicates a more stable suspension. When the zeta potential is high, colloidal particles with similar charges experience electrostatic repulsion, preventing their aggregation or clustering. On the other hand, as the electric potential decreases (lower zeta potential), the particles tend to come closer together, leading to their aggregation and potential instability [40].

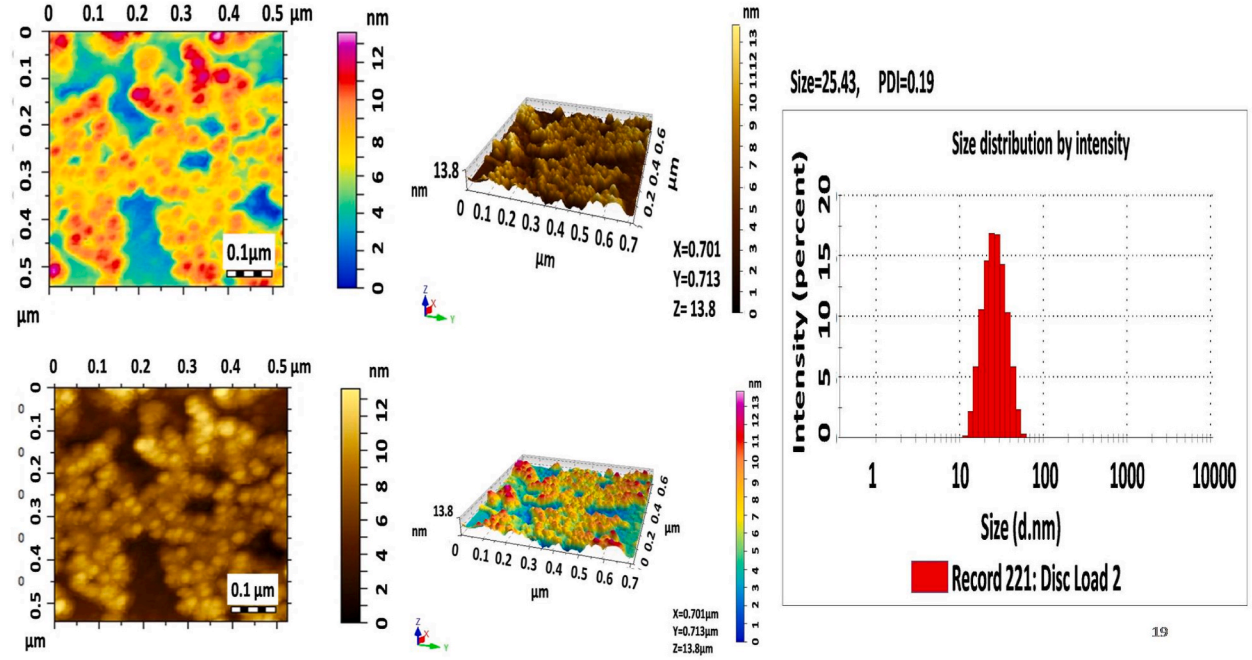

Fig. 4. Images of AgNPs/HA by atomic force microscopy and zeta sizer graph shows size of AgNPs/HA approximately 25 nm with low PDI value 0.19 and spherical shape.

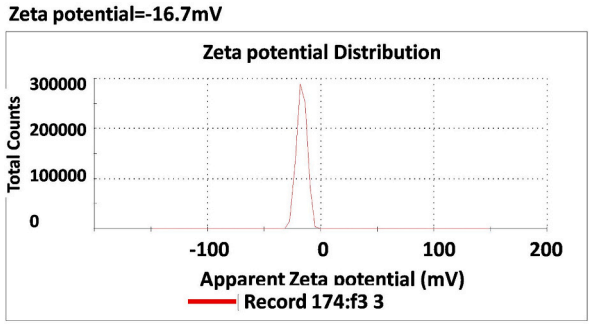

Fig. 5. Zeta potential of AgNPs/HA shows highly negative value −16 mV.

3.3. XRD pattern of AgNPs/HA

The XRD pattern AgNPs and AgNPs/HA were studied (Fig. 6a and b). The XRD pattern of AgNPs/HA exhibited distinct diffraction peaks at various 2θ values, including 27.7, 32.2, 33.7, 37.7, 39.7, 44.5, 52.2, 55.0, 56.9, 64.8, and 71.9° (Fig. 6b) These peaks indicate the presence of a crystalline and FCC structure within the synthesized AgNPs/HA. Moreover, the presence of sharp and intense peaks signifies the high purity of the synthesized AgNPs/HA, indicating minimal impurities or contaminants. The XRD analysis confirms the successful formation of AgNPs/HA with the desired crystalline structure. Martínez et al. [45] studied the XRD pattern at $2\,\theta = 37.043$ and 40.3 shows crystalline and FCC structure of AgNPs. X-ray crystallography was employed to verify the structures of HA and the synthesized AgNPs. The diffraction patterns were obtained in the range of 0°–80° for both samples. The XRD pattern of HA showed strong peaks at angles (2) 46, 64, and 72, demonstrating the substance's crystalline structure. The presence of HA on the surface of AgNPs was evidenced by the appearance of two additional peaks around angles 32 and 44 (Fig. 6a), which were not assigned specific values. These peaks suggest the presence of interactions between HA and the AgNPs, indicating the coating of HA on the surface of the NPs. The results of this study align with the findings reported in literature regarding the presence of a crystalline structure within HA and AgNPs/HA. Both studies observed distinct diffraction peaks, indicating the crystalline nature of the samples. The presence of specific peaks in the XRD patterns suggests well-defined crystal lattices. Dantas et al. [40] discussed the effect of HA as a stabilizing agent, suggesting a more amorphous structure in HA-coated AgNPs. The XRD analysis confirms the successful formation of AgNPs/HA with the desired crystalline structure and provides insights into the influence of HA on the crystallinity of the synthesized nanoparticles.

3.4. Antibacterial studies

The antibacterial activities of AgNPs/HA and AgNPs as evaluated by the disk diffusion method, as shown in Tables 1 and 2. The disks with concentrations of 0.156, 0.312, and 0.625 mg/mL in agar plate that were kept in an incubator for 24 h did not exhibit any zones of inhibition, and bacterial growth was evident. AgNP concentrations of 1.25, 2.5, and 5 mg/mL on disks displayed inhibitory zones, clearly inhibiting bacterial growth (Fig. 7). Additionally, same quantities were introduced to culture media tubes containing bacteria for the purpose of determining MBC, and after 24 h of incubation, the lack of turbidity revealed that these concentrations were MBC. AgNPs/HA, displayed an inhibitory zone at concentrations of 2.5 and 5 mg/mL; their MBC was determined using the broth macro dilution method (Fig. 7). AgNPs and AgNPs/HA produced more pronounced results because of their larger sizes, as reported [44,46]. The result of another study the MIC of AgNPs is 0.625 mg/l the size of AgNPs is 5 nm [42]. When we compare all these studies and present study it showed that antimicrobial activity of AgNPs depends upon size and sources and nature of microorganisms. It was also reported that small sized AgNPs with spherical shape shown more antimicrobial activity due to large surface area [47]. Fig. 8 shows the differences in the antimicrobial activity of silver nanoparticles coated with humic acid at various concentrations against the microorganisms tested. The AgNPs/HA showed the highest level of antimicrobial activity against *streptococcus pyogeneses* while lowest level of antimicrobial activity against *salmonella typhi*on the other hand, there was no observable antimicrobial activity in the tested colonies at concentrations of 0.156, 0.312, 0.626 and 1.25 mg/mL. This graph illustrates the varying antimicrobial activity of silver nanoparticles at different concentrations against the tested microorganisms. Streptococcus pyogeneses exhibited the highest amount of antimicrobial activity, whereas Salmonella typhi exhibited the lowest level of antimicrobial activity. However, at doses of 0.156 g/mL, 0.3 g/mL, and 0.626 g/mL, no antibacterial activity was found in the tested colonies (Fig. 9). E. coli and S. aureus had minimum bactericidal concentrations (MBCs) of 25 g/mL and 100 g/mL, respectively, and minimal inhibitory concentrations (MICs) of 6.25 g/mL and 50 g/mL, respectively. Huq et al. [19] demonstrated the minimum bactericidal concentrations (MBCs) of Pseudomonas aeruginosa and Staphylococcus aureus were 50 and 200 g/mL, respectively, while the minimal inhibitory concentrations (MICs) of both bacteria were 100 g/mL and 6.25 g/mL.

4. Conclusion

This study involved the synthesis of AgNPs coupled with humic acid extracted from cow dung. The resulting AgNPs-HA complexes

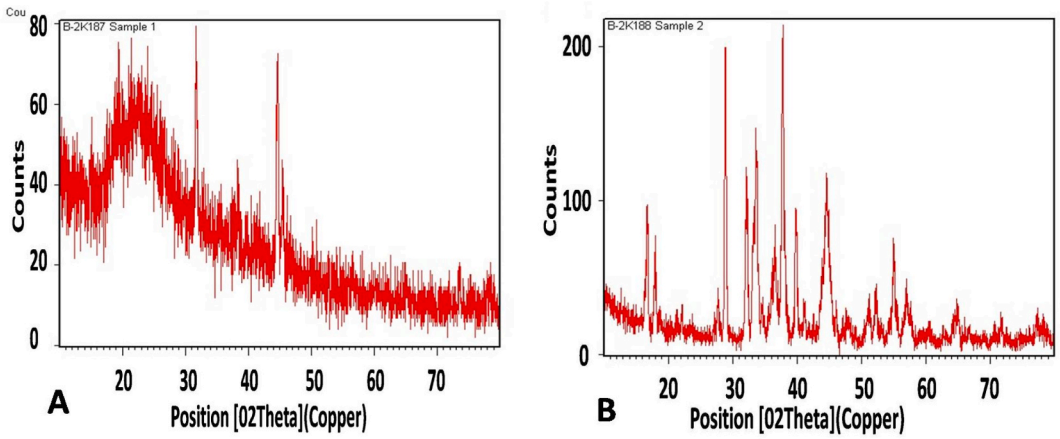

Fig. 6. (a) XRD pattern shows crystalline and fcc structure of humic acid. (b) XRD pattern shows crystalline and fcc structure of AgNPs/HA and interaction of humic acid with AgNPs.

Table 1
AgNPs in different concentration ranging from 0.156 mg/mL −5 mg/mL for the determination of antibacterial activity.

Bacteria	Concentration of AgNPs ranging from 0.156 mg to 5mg/mL					
	0.156 mg/ml	0.312 mg/mL	0.625 mg/ml	1.25 mg/mL	2.5 mg/mL	5 mg/mL
Staphylococcus aureus	0.0 mm	0.0 mm	0.0 mm	9.0 mm	12.0 mm	16.0 mm
Streptococcus pyogenes	0.0 mm	0.0 mm	0.0 mm	10.0 mm	12.0 mm	17.0 mm
E. coli	0.0 mm	0.0 mm	0.0 mm	8.0 mm	11.0 mm	13.0 mm
Pseudomonas	0.0 mm	0.0 mm	0.0 mm	8.0 mm	12.0 mm	14.0 mm
Salmonella typhi	0.0 mm	0.0 mm	0.0 mm	6.0 mm	9.0 mm	13.0 mm

Table 2
AgNPs/HA in different concentration ranging from 0.156 mg to 5mg/mL for the determination of antibacterial activity

Bacteria	Concentration of AgNPs/HA ranging from 0.156 mg to 5mg/ml					
	0.156 mg/mL	0.312 mg/mL	0.625 mg/mL	1.25 mg/mL	2.5 mg/mL	5 mg/mL
Staphylococcus aureus	0.0 mm	0.0 mm	0.0 mm	0.0 mm	10.0 mm	14.0 mm
Streptococcus pyogenes	0.0 mm	0.0 mm	0.0 mm	0.0 mm	9.0 mm	14.0 mm
E.coli	0.0 mm	0.0 mm	0.0 mm	0.0 mm	8.0 mm	13.0 mm
Pseudomonas aeruginosa	0.0 mm	0.0 mm	0.0 mm	0.0 mm	8.0 mm	12.0 mm
Salmonella typhi	0.0 mm	0.0 mm	0.0 mm	0.0 mm	7.0 mm	10.0 mm

were then assessed for their antimicrobial activity against various gram-positive and gram-negative bacterial strains. AgNPs coupled with HA was characterized by techniques UV–vis, FT-IR, XRD, AFM, and zeta potential. AgNPs/HA average size of 25.34 nm and spherical shape with 0.19 low polydispersity index (PDI) was confirmed. The zeta potential value −16.7 mV, indicated the stability of AgNPs/HA. Moreover, for future medical application its stability was confirmed with different items at different concentration of blood plasma, salt, and pH levels for over 90 days. Subsequently, broad spectrum antimicrobial activity of AgNPs/HA against *Staphylococcus, Streptococcus, E. coli, Pseudomonas, and S. typhi*was determined and found highly active against *Streptococcus,* while less active against *S. Typhi*. The 2.5 and 5 mg/mL concentration were determined as MBC for AgNPs and AgNPs/HA respectively. The study revealed that AgNPs coated with HA exhibited enhanced antimicrobial activity against a range of microorganisms. This improved efficacy is likely due to the therapeutic potential of humic acid-coated nanoparticles, making them a promising tool in the fight against microbial infections.

CRediT authorship contribution statement

Shabir Ahmed Dharejo: Writing – original draft, Methodology, Investigation, Formal analysis, Data curation. **Tajnees Pirzada:** Writing – review & editing, Supervision, Software, Project administration, Methodology. **Muhammad Raza Shah:** Writing – review & editing, Supervision, Project administration, Formal analysis. **Ahmed Nadeem:** Writing – review & editing, Software, Resources, Investigation, Formal analysis, Conceptualization. **Khalid Hussain Thebo:** Writing – review & editing, Software, Investigation, Formal analysis.

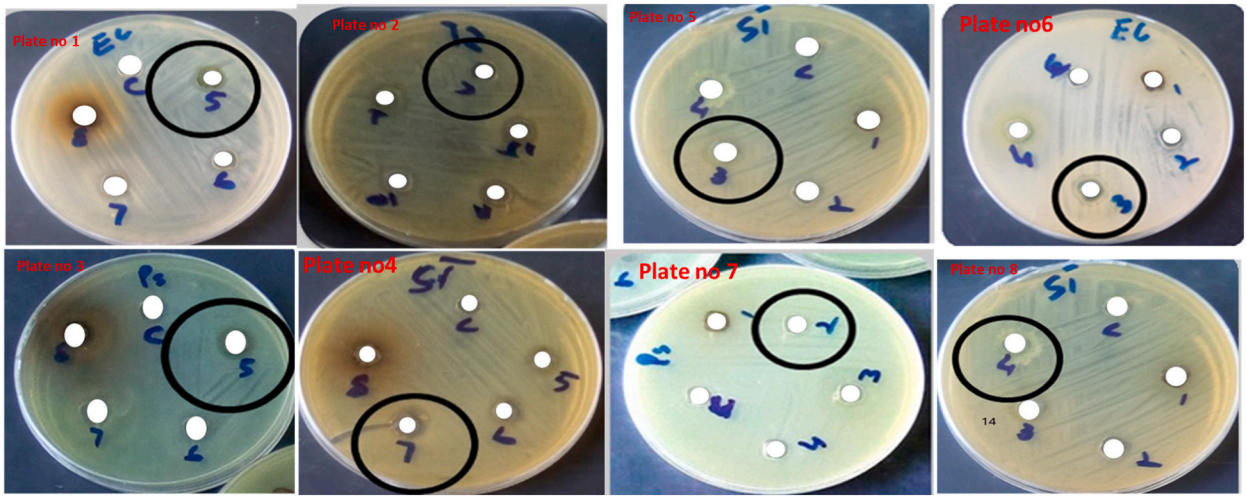

Fig. 7. illustrates the inhibition zones for various microbes. Plates 1 to 4 display the inhibition zones caused by AgNPs, while plates 5 to 8 show the inhibition zones caused by AgNPs/HA, respectively.

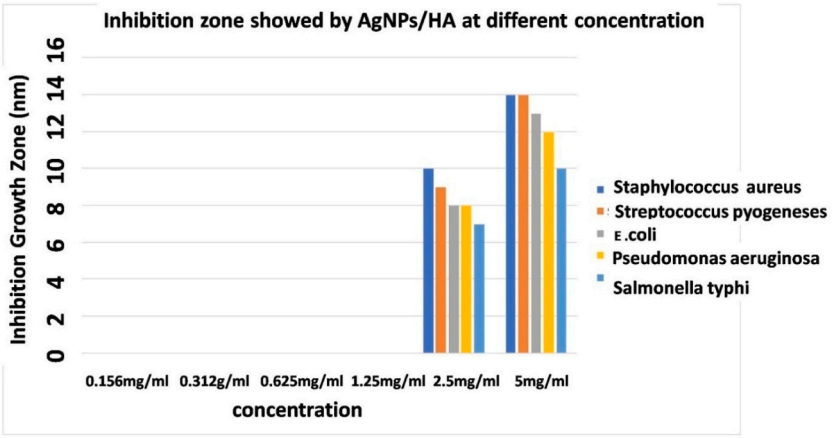

Fig. 8. Graphical representation of antimicrobial activity of AgNPs at different concentration ranging from 0.156 mg/mLto 5 mg/mL. It shows highest antimicrobial activity against *Streptococcus pyogeneses* and lowest against *Salmonella typhi.*

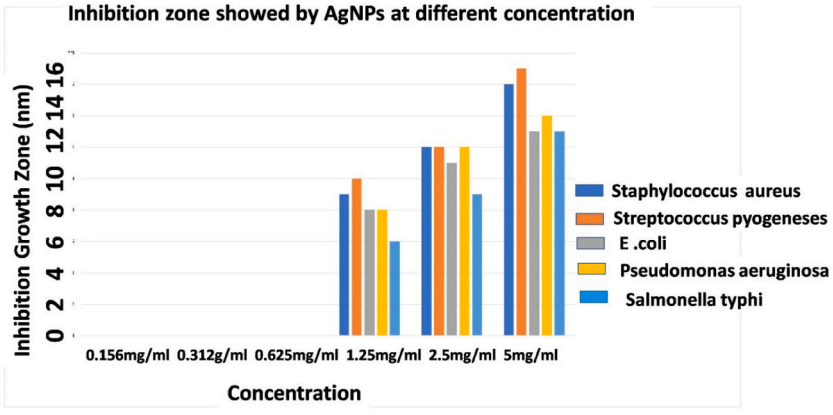

Fig. 9. Graphical representation of antimicrobial activity of AgNPs at different concentration ranging from 0.156 mg/mL to 5 mg/mL. It shows highest antimicrobial activity against *Streptococcus pyogeneses* and lowest against *Salmonella typhi.*

Data accessibility

All data generated and analyzed in this study have been included in this published article and are available upon reasonable request.

Declaration of competing interest

The authors declare that they have no known competing financial interests or personal relationships that could have appeared to influence the work reported in this paper.

Acknowledgments

The authors acknowledge and extend their appreciation to the Researchers Supporting Project Number (RSP2025R124), King Saud University, Riyadh, Saudi Arabia. Authors are also thankful for Shah Abdul Latif University Khairpur Mir's for research support.

References

[1] S.A. Al-Mutwalli, et al., Intensification of adsorptive ceramic ultrafiltration membrane system by nanoclay coating and multivariate optimization of humic acid removal, Journal of Water Process Engineering 68 (2024) 106388.
[2] V. Nitin, et al., Properties of humic acid substances and their effect in soil quality and plant Health, in: M. Abdelhadi (Ed.), Humus and Humic Substances, IntechOpen, Rijeka, 2022. Ch. 4.
[3] Y. Ding, et al., Binding characteristics of heavy metals to humic acid before and after fractionation by ferrihydrite, Chemosphere 226 (2019) 140–148.
[4] Y. Wang, et al., Enhanced local CO coverage on Cu quantum dots for boosting electrocatalytic CO2 reduction to ethylene, Adv. Funct. Mater. (2024) 2417764.
[5] J. Xie, et al., One-dimensional consolidation analysis of layered unsaturated soils: an improved model integrating interfacial flow and air contact resistance effects, Comput. Geotech. 176 (2024) 106791.
[6] F. de Souza, S.R. Bragança, Extraction and characterization of humic acid from coal for the application as dispersant of ceramic powders, J. Mater. Res. Technol. 7 (3) (2018) 254–260.
[7] K. Zhang, et al., Water quality impact on fish behavior: a review from an aquaculture perspective, Rev. Aquacult. 17 (1) (2025) e12985.
[8] I.V. Efimova, S.L. Khil'ko, O.V. Smirnova, Antioxidant activity of humic acids in radical-chain oxidation processes, Russ. J. Appl. Chem. 85 (9) (2012) 1351–1354.
[9] B.G. Mvila, et al., Synthesis and characterization of a stable humic-urease complex: application to barley seed encapsulation for improving N uptake, J. Sci. Food Agric. 96 (9) (2016) 2981–2989.
[10] Y. Lai, et al., An antibiotic-free platform for eliminating persistent Helicobacter pylori infection without disrupting gut microbiota, Acta Pharm. Sin. B 14 (7) (2024) 3184–3204.
[11] S. Majeed, et al., Bioengineering of green-synthesized TAT peptide-functionalized silver nanoparticles for apoptotic cell-death mediated therapy of breast adenocarcinoma, Talanta 253 (2023) 124026.
[12] H. Barabadi, et al., Chapter 11 - functionalized bioengineered metal-based nanomaterials for cancer therapy, in: H. Barabadi, E. Mostafavi, C. Mustansar Hussain (Eds.), Functionalized Nanomaterials for Cancer Research, Academic Press, 2024, pp. 219–260.
[13] G. Feng, et al., Novel (Ni, Mn) co-doping CuFe5O8 black ceramic pigment with pinning strengthen effect in high-temperature black zirconia ceramic application, Ceram. Int. (2024), https://doi.org/10.1016/j.ceramint.2024.12.186.
[14] Y. Luo, et al., Novel multidimensional composite development for aging resistance of SBS-modified asphalt by attaching zinc oxide on expanded vermiculite, Energy & Fuels 38 (17) (2024) 16772–16781.
[15] E. Sánchez-López, et al., Metal-based nanoparticles as antimicrobial agents: an overview, Nanomaterials 10 (2) (2020) 292.
[16] X. Wang, et al., Probiotic-Mediated biosynthesis of silver nanoparticles and their antibacterial applications against pathogenic strains of Escherichia coli O157: H7, Polymers (Basel) 14 (9) (2022) 1834.
[17] N. Nan, et al., A stretchable, highly sensitive, and multimodal mechanical fabric sensor based on electrospun conductive nanofiber yarn for wearable electronics, Advanced Materials Technologies 4 (3) (2019) 1800338.
[18] H. Samadian, et al., Genotoxicity assessment of carbon-based nanomaterials; Have their unique physicochemical properties made them double-edged swords? Mutation Research/Reviews in Mutation Research 783 (2020) 108296.
[19] M.A. Huq, Green synthesis of silver nanoparticles using pseudoduganella eburnea MAHUQ-39 and their antimicrobial mechanisms investigation against drug resistant human pathogens, Int. J. Mol. Sci. 21 (4) (2020) 1510.
[20] H. Zhou, et al., Highly efficient preparation of crystalline yttrium carbonate in sodium carbonate system: formation and growth mechanism, J. Rare Earths (2024), https://doi.org/10.1016/j.jre.2024.08.013.
[21] S. Akter, M.A. Huq, Biologically rapid synthesis of silver nanoparticles by Sphingobium sp. MAH-11(T) and their antibacterial activity and mechanisms investigation against drug-resistant pathogenic microbes, Artif. Cells, Nanomed. Biotechnol. 48 (1) (2020) 672–682.
[22] Gao, X., et al., When it's heavier: interfacial and solvation chemistry of isotopes in aqueous electrolytes for Zn-ion batteries. Angew. Chem. Int. Ed., 2023. 62 (16): p. e202300608.
[23] X. Chen, P. Feng, X. Li, High reactivity of dimethyl ether activated by zeolite ferrierite within a fer cage: a prediction study, Molecules 29 (9) (2024) 2000.
[24] M.A. Huq, S. Akter, Biosynthesis, characterization and antibacterial application of novel silver nanoparticles against drug resistant pathogenic Klebsiella pneumoniae and Salmonella enteritidis, Molecules 26 (19) (2021) 5996.
[25] S. Sharif, et al., Functionalised graphene oxide-based nanofiltration membranes with enhanced molecular separation performance, Mater. Res. Innovat. (2021) 1–9.
[26] S. Hussain, et al., Synthesis and characterization of ZnO/samarium-doped ceria nanocomposites for solid oxide fuel cell applications, Ionics 27 (11) (2021) 4849–4857.
[27] B.-L. Sun, et al., Ultrahigh-strength textile fiber-supported schiff base copper complexes for photocatalytic degradation of methyl orange, ACS Appl. Polym. Mater. 6 (21) (2024) 13077–13088.
[28] J. Khan, et al., Antioxidant, antimicrobial, and photocatalytic potential of cobalt fluoride (CoF_2) nanoparticles, Adsorpt. Sci. Technol. 2022 (2022) 9369201.
[29] X. Ji, et al., Toward enhanced aerosol particle adsorption in never-bursting bubble via acoustic levitation and controlled liquid compensation, Adv. Sci. 10 (19) (2023) 2300049.
[30] T. Zhang, et al., Ultrahigh-Performance fiber-supported iron-based ionic liquid for synthesizing 3,4-dihydropyrimidin-2-(1H)-ones in a cleaner manner, Langmuir 40 (18) (2024) 9579–9591.
[31] F. Soomro, et al., Highly efficient nickel fluoride nanoparticles with enhance electrochemical properties, Inorg. Chem. Commun. 155 (2023) 111023.
[32] M.M.A.T. Tajnees Pirzada, Mohammad Raza Shah, Analysis of humic acids isolated from agriculture soils, J. Chem. Soc. Pakistan 34 (6) (2012) 1594–1600.

[33] S.A.A. Omid Shabnani Moghadam, Arash Hemati, Azarian Journal of Agriculture Determining the best extractant and extraction conditions for fulvic acid through qualitative and quantitative analysis of vermicompost, Azarian Journal of Agriculture (2) (2015) 75–80.
[34] Y. Hao, et al., Humic acid assisted chemical synthesis of silver nanoparticles for inkjet printing of flexible circuits, J. Mater. Sci. Mater. Electron. 30 (23) (2019) 20400–20409.
[35] F.-A. Juan Carlos, et al., Antimicrobial poly (methyl methacrylate) with silver nanoparticles for dentistry: a systematic review, Appl. Sci. 10 (11) (2020) 4007.
[36] G. Barančíková, N. Senesi, G. Brunetti, Chemical and spectroscopic characterization of humic acids isolated from different Slovak soil types, Geoderma 78 (3) (1997) 251–266.
[37] A. Behboudi, Y. Jafarzadeh, R. Yegani, Enhancement of antifouling and antibacterial properties of PVC hollow fiber ultrafiltration membranes using pristine and modified silver nanoparticles, J. Environ. Chem. Eng. 6 (2) (2018) 1764–1773.
[38] Y. Hao, et al., Thermal decomposition of allyl-imidazolium-based ionic liquid studied by TGA–MS analysis and DFT calculations, Thermochim. Acta 501 (1) (2010) 78–83.
[39] L. Wang, et al., Characterization, antioxidant and antimicrobial activities of green synthesized silver nanoparticles from Psidium guajava L. leaf aqueous extracts, Mater Sci Eng C Mater Biol Appl 86 (2018) 1–8.
[40] K.N.M. Dantas, et al., Antimycotic nail polish based on humic acid-coated silver nanoparticles for onychomycosis, Journal of Chemical Technology & Biotechnology 96 (8) (2021) 2208–2218.
[41] V. Vadlapudi, R. Amanchy, Phytofabrication of silver nanoparticles using Myriostachya wightiana as a novel bioresource, and evaluation of their biological activities, Braz. Arch. Biol. Technol. 60 (2017) e17160329.
[42] P. Singh, I. Mijakovic, Strong antimicrobial activity of silver nanoparticles obtained by the green synthesis in viridibacillus sp. extracts, Front. Microbiol. 13 (2022) 820048.
[43] E.C.R. Lopez, et al., Humic acid functionalized - silver nanoparticles as nanosensor for colorimetric detection of copper (II) ions in aqueous solutions, Key Eng. Mater. 831 (2020) 142–150.
[44] N.S. Alduraihem, et al., Anticancer and antimicrobial activity of silver nanoparticles synthesized from pods of Acacia nilotica, Processes 11 (2) (2023) 301.
[45] J.C. Martínez Espinosa, et al., Characterization of silver nanoparticles obtained by a green route and their evaluation in the bacterium of Pseudomonas aeruginosa, Crystals 10 (5) (2020) 395.
[46] S. Devanesan, M.S. AlSalhi, Green synthesis of silver nanoparticles using the flower extract of abelmoschus esculentus for cytotoxicity and antimicrobial studies, Int J Nanomedicine 16 (2021) 3343–3356.
[47] I.X. Yin, J. Zhang, I.S. Zhao, The Antibacterial Mechanism of Silver Nanoparticles and its Application in Dentistry, vol. 15, 2020, pp. 2555–2562.